ARTICLE   OPEN

Check for updates

Predictability of Indian Ocean precipitation and its North Atlantic teleconnections during early winter

Muhammad Adnan Abid [1,2 ✉], Fred Kucharski[1,2], Franco Molteni[3] and Mansour Almazroui[2,4]

The Tropical Western-Central Indian Ocean (WCIO) precipitation anomalies play an important role in modulating the anomalous climate conditions in the North Atlantic and European (NAE) region during the early boreal winter (November–December; ND) season. In this study, we analyzed the forcing mechanism and predictability for the early winter tropical WCIO precipitation anomalies and its teleconnections to the North Atlantic region. The two main forcing mechanisms emerging are the autumn Indian Ocean Dipole (IOD) and a direct atmospheric teleconnection from El Niño-Southern Oscillation (ENSO). Since the autumn IOD is partially forced by ENSO, their independent contributions are also investigated. We found the IOD dominates over the ENSO contribution. The ECMWF-SEAS5 seasonal re-forecast reproduces these forcing mechanisms well and shows a substantial prediction skill for early winter WCIO precipitation. Moreover, the North Atlantic response to the positive WCIO phase projects spatially onto the positive North Atlantic Oscillation (NAO) phase through atmospheric teleconnections and leads to warming in central and western Europe. This teleconnection is reproduced by ECMWF-SEAS5, but with weaker amplitude. Moreover, a significant prediction skill for the NAO as well as for the central and western European temperature anomalies is noted, which is mostly induced by the Indian Ocean precipitation anomalies during early winter.

INTRODUCTION

Understanding the mechanism for the North Atlantic Oscillation (NAO)[1] predictability that modulates and favors the extreme climatic conditions in the North Atlantic European (NAE) region is important. In recent decades, the warming in the Indian Ocean favors frequent positive NAO[2–5] conditions, which leads to mild winters over the NAE region[6], particularly during early winter (November–December) when the Indian Ocean (IO) teleconnection dominates over the direct teleconnection from El Niño-Southern Oscillation (ENSO)[7,8].

Tropical Indian Ocean (TIO) interacts with the other oceanic basins through atmospheric and oceanic pathways[9–12]. There are two main modes of variability in the Indian Ocean, one is the Indian Ocean Basin Mode (IOBM) and the other is the Indian Ocean dipole (IOD). Both modes modulate the global climate variability on different timescales[13–16] and show strong seasonality. The IOBM is forced by the El Niño-Southern Oscillation (ENSO) and peaks in boreal spring following an ENSO event, whereas the IOD peaks and shows maximum variability in boreal autumn[10]. The IOD is defined as the see-saw of the Sea Surface Temperatures (SSTs) anomalies between the western and the southeastern Indian Ocean[17]. ENSO, through an atmospheric bridge, also strongly interacts with the IOD mode[18]. ENSO influences IOD due to an anomalous walker circulation, which induces a low-level easterly flow that shallows the thermocline over the eastern TIO which, in turn, strengthens the warm pool over the western Indian Ocean during a warm ENSO event, favoring the positive IOD phase. The ENSO-IOD relationship peaks during the boreal autumn season[16], but still about half of IOD variability can exist independently. Recently, a very strong IOD event developed during boreal autumn and early winter of 2019/20, favoring the positive NAO phase during boreal winter that led

to extreme warm and wet climatic conditions over the North Atlantic and European (NAE) region[6] and drought-like conditions that led to the extreme fires during the Australian summer season in the southern hemisphere[19]. In general, Indian Ocean precipitation anomalies induced by SST anomalies in the Indian Ocean and ENSO region are important tropical sources for the eastward propagating wave from the Indian Ocean leading to anomalous atmospheric circulation anomalies in the NAE region[7,8,20]. Several studies investigated the IOD predictability[21,22], but limited information is available about the prediction skill of the precipitation anomalies in the Indian Ocean. In the current study, we used ECMWF-SEAS5 re-forecast data[23] to investigate the prediction skill of the Indian Ocean precipitation anomalies as well as for the NAE circulation anomalies in early boreal winter.

The importance of Indian Ocean induced NAE circulation anomalies during the boreal winter season has been recognised as an important source of predictability in coupled Ocean-Atmosphere models on sub-seasonal to seasonal timescales[24–29]. A considerable effort has been made to diagnose the Indian Ocean teleconnections in coupled models[24,26], but how well the models are capable in predicting the precipitation anomalies in the Indian Ocean during the boreal early winter season is not well documented, which is thus investigated in the current study. In the NAE region, NAO modulates the atmospheric circulation anomalies and the surface anomalous conditions during boreal winter[30]. However, the NAO prediction skill is limited during boreal winter (December-February) compared to the Pacific North American (PNA) skill, mainly due to a weaker ENSO teleconnection[31–35]. Nonetheless, there is some moderate predictability for the NAO[36] forced by the tropical oceans[37], transmitted through tropospheric[7,38–41] and stratospheric pathways[42–47]. An interesting aspect of the NAO prediction skill is that its actual prediction skill

[1]Earth System Physics, Abdus Salam International Centre for Theoretical Physics (ICTP), Trieste, Italy. [2]Centre of Excellence for Climate Change Research (CECCR)/Department of Meteorology, King Abdulaziz University, Jeddah, Saudi Arabia. [3]European Centre for Medium-Range Weather Forecasts (ECMWF), Reading, UK. [4]Climatic Research Unit, School of Environmental Sciences, University of East Anglia, Norwich, UK. ✉email: mabid@ictp.it
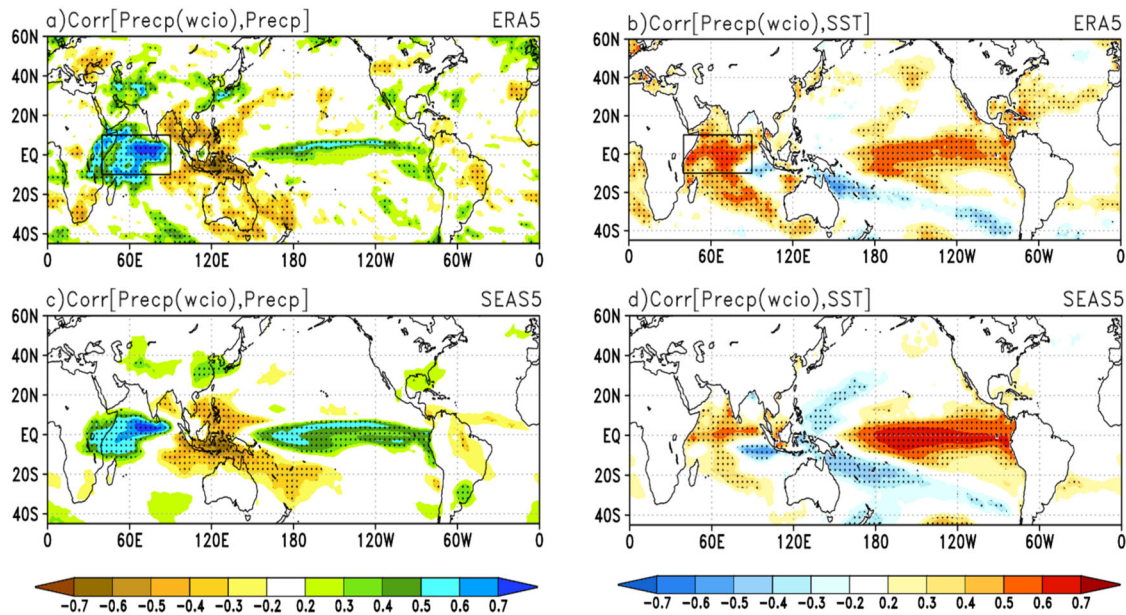
Fig. 1 Western-Central Indian Ocean (WCIO) precipitation anomalies relationship with precipitation and SSTs. a Correlation of the western-central Indian Ocean (WCIO) precipitation anomalies with the global Precipitation during early winter (November-December; ND); (**b**) same as of (**a**) but with the global Sea Surface Temperature (SST) anomalies; (**c, d**). same as of (**a, b**) but for the ECMWF-SEAS5 dataset. Stippling denotes statistical significance at 95% confidence level.

is larger than the potential predictability estimated from the model ensembles, which leads to the signal-to-noise paradox[48]. This could partly be related to the substantial variations in the tropical ENSO teleconnections to the NAO from early to late winter[7,39,40], where in early winter the tropical Indian Ocean mediates the ENSO teleconnection, resulting in a complex interference of signals, where in-phase ENSO and Indian Ocean forcing tends to enhance the variability of the circulation anomalies in the NAE region[7,8].

Therefore, in the current study, we assessed the predictability of the tropical Indian Ocean precipitation anomalies and its teleconnections to the North Atlantic and European (NAE) region during early winter using observational and ECMWF-SEAS5 seasonal re-forecast dataset for the period 1981–2019.

RESULTS

Tropical Indian Ocean variability during late fall to early winter

The tropical western-central Indian Ocean precipitation anomalies are well connected with ENSO[7,25,49] during early (ND) winter. To analyze the precipitation anomalies in this region, we define an area-averaged precipitation anomaly index over the IO region [40:90°E; 10°S:10°N], referred hereinafter as the Tropical Western-Central Indian Ocean (WCIO) index. Figure 1a, b show the contemporaneous WCIO precipitation index correlation with global precipitation and SSTs, respectively. Apart from the large local Indian Ocean positive correlations (about 0.6), also large positive correlations appear in the central-eastern equatorial Pacific, which resemble ENSO-related anomalies. ENSO may impact WCIO precipitation in two ways: A direct early winter atmospheric bridge and through autumn IOD SST perturbations[12]. Indeed, the IOD-Niño3.4 link peaks in the boreal autumn in observations, which is also represented well in the ECMWF-SEAS5 (Supplementary Fig. 1). The ECMWF-SEAS5 re-forecast also reproduces the observed WCIO precipitation and SST co-variances quite well during early winter (Fig. 1c, d).

To test the hypothesis of a dual ENSO and IOD forcing further, in Fig. 2a, scatterplots of the observed early winter (ND) WCIO

precipitation with the contemporaneous Niño3.4, and with October IOD indices are shown. There is a clear positive and statistically significant relationship noted between the WCIO index and the contemporaneous Niño3.4 index (black circles) as well as with October IOD (red triangles) with correlations of 0.53 and 0.71, respectively (statistically significant at 95% confidence level). Based on the regression coefficients, the precipitation anomalies in the western IO are more sensitive (slope in scatter plot) to the pre-conditioning of the autumn (October) IOD (0.92 mm/day/K) compared to the contemporary Niño3.4 (0.43 mm/day/K), which is almost double for IOD compared to ENSO. It confirms that ENSO directly impacts the WCIO precipitation through an atmospheric bridge, but also indirectly through the autumn IOD conditions. Moreover, this result also suggests that IOD could impact the WCIO precipitation independently from ENSO. The ECMWF-SEAS5 reproduces these relationships reasonably well, with stronger correlations, but with less sensitivity, regarding the October IOD-WCIO precipitation relationship (Fig. 2b).

Next, we estimated the lead-lag correlation of bi-monthly overlapping seasons of the WCIO precipitation anomalies with the October IOD index and early winter (ND) Niño3.4 SSTs index. In order to establish the independent responses of IOD and ENSO to the WCIO precipitation, we have removed statistically the impact of early winter (ND) Niño3.4 SSTs from the global SSTs and re-calculated the residual IOD index for October using the partial regression[49,50] (see "methods"). The resulting index will refer as partial IOD (PIOD)$_{noNiño34}$. Similarly, we removed the October IOD SSTs influence from global SSTs to re-estimate the residual early winter (ND) Niño3.4 index, referred to as (PNiño34)$_{noIOD}$ in the following. Figure 3a shows the correlation of IOD and (PIOD)$_{no-Niño34}$ with WCIO precipitation for bi-monthly overlapping seasons October-November (ON) to February-March (FM). Overall, there is no significant change noted for the (PIOD)$_{noNiño34}$ index (black solid lines with circles) compared to the full IOD (red solid lines with stars) relationship with WCIO precipitation. However, the situation is different, for the (PNiño34)$_{noIOD}$ index used instead of the full Niño3.4 index (Fig. 3b). In this case the (PNiño34)$_{noIOD,}$ correlation with WCIO drops considerably to statistically insignif-icant values (black solid lines with circles) compared to full Niño3.4
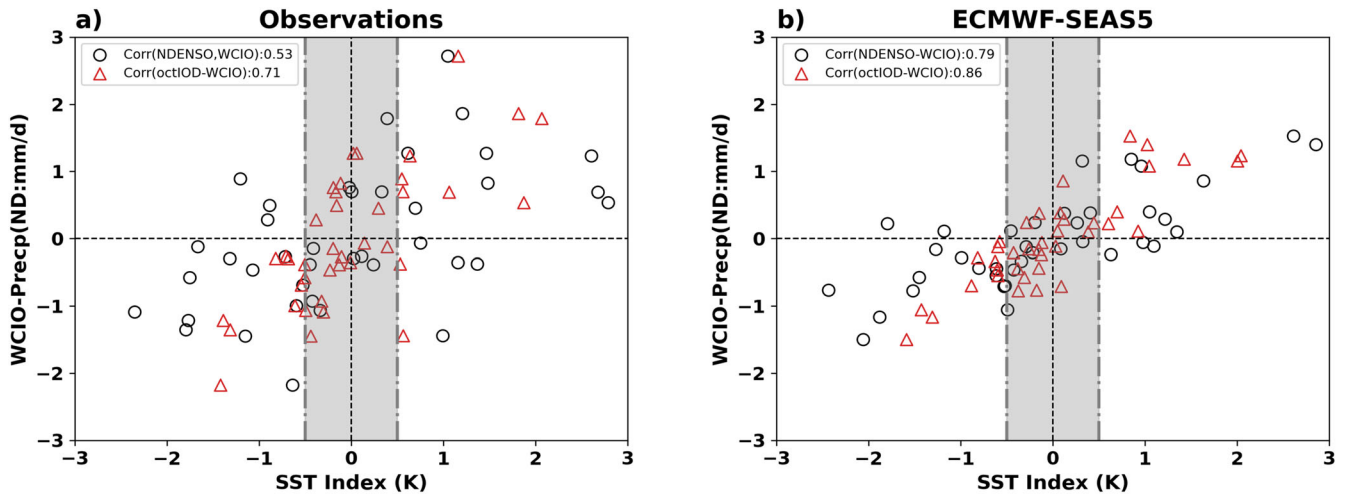
Fig. 2 ENSO vs IOD relationship with WCIO precipitation anomalies. a Observed Scatter plots for the early winter (November–December; ND) WCIO precipitation with the November–December (ND) Niño3.4 (black open circles) and October IOD (red triangles) SST based indices. The grey shaded region corresponds to ±0.5 K SST anomalies. Correlation Coefficient (CC) of ND-WCIO precipitation index and ENSO(IOD) SST index is 0.53 (0.71) and slope is 0.43 (0.92) mmd^{-1}/K; (**b**) same as of panel (**a**) but for ECMWF-SEAS5, CC between ND-WCIO precipitation and ENSO(IOD) is 0.79 (0.86) while the slope is 0.43 (0.75) mmd^{-1}/K.
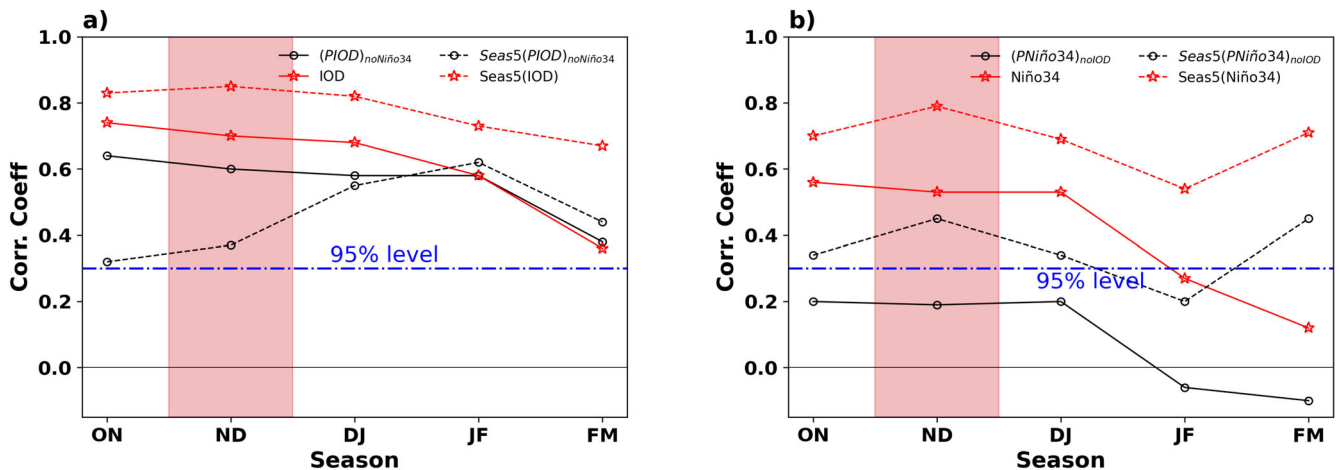

Fig. 3 Role of constructive interference of IOD and ENSO in WCIO precipitation anomalies. a Observed October IOD index (based on SST) lag Correlation Coefficient (CC) with the western-central Indian Ocean (WCIO) precipitation anomalies in 2-months overlapping season for the period 1981–2019 (red solid line with star). Same but with linearly independent October-IOD $(PIOD)_{noNiño34}$ are shown in black solid line (with circle); Corresponding lines for ECMWF-SEAS5 are shown in dashed lines; (**b**) Same as panel (**a**), except using ND (November-December) Niño3.4 SST index (red solid and dashed lines) and linearly independent ND-Niño34 $(PNiño34)_{noIOD}$ (black solid and dashed lines). Blue line indicates the statistical significance of the CC at 95% confidence level.

(red solid lines with stars). This indicates that IOD is the key mechanism linking ENSO to WCIO precipitation, but also suggests that the IOD may impact WCIO precipitation independently of ENSO. If both ENSO and IOD interfere constructively, then the WCIO precipitation shows the strongest response. Also, the ECMWF-SEAS5 re-forecast shows a similar behavior as of observations, where strongest impact is noted with constructive interference of ENSO and IOD (dashed lines in Fig. 3). However, the drop in correlations for $(PIOD)_{noNiño34}$ is larger compared to the $(PNiño34)_{noIOD}$ in the model compared to observations. The large drop in Pure IOD relationship in ECMWF-SEAS5 compared to observations is likely because of model biases in simulating the IOD spatial structure and its relation to precipitation anomalies in the Indian Ocean, where the zonal maxima of the IOD is shifted to the eastern IO (Supplementary Fig. 2c, d) compared to the observations (Supplementary Fig. 2a, b).

Tropical Indian Ocean teleconnections to the NAE region

In order to analyze the NAE circulation anomalies mediated through Indian Ocean heating anomalies, we regress the 200-hPa geopotential height (Z200), Mean Sea Level Pressure (MSLP), 850-hPa temperature anomalies and Surface Air Temperature (SAT) onto the standardized WCIO precipitation anomalies index during early winter. The response to a positive WCIO precipitation index projects spatially onto the positive NAO phase in the North Atlantic region (Fig. 4a, b) and the related temperature advection leads to a substantial warming in the European continent[51] (Fig. 4c), which also appears in the Surface Air Temperature (SAT) regression maps over the NAE, with a significant response over the western European region (Fig. 4d). The ECMWF-SEAS5 re-forecast reproduces the NAO pattern (Fig. 4e, f) and the low-level warming well (Fig. 4g), but with reduced magnitudes compared to observations. Moreover, the anomalous increase in the surface temperatures over the western European region is also well
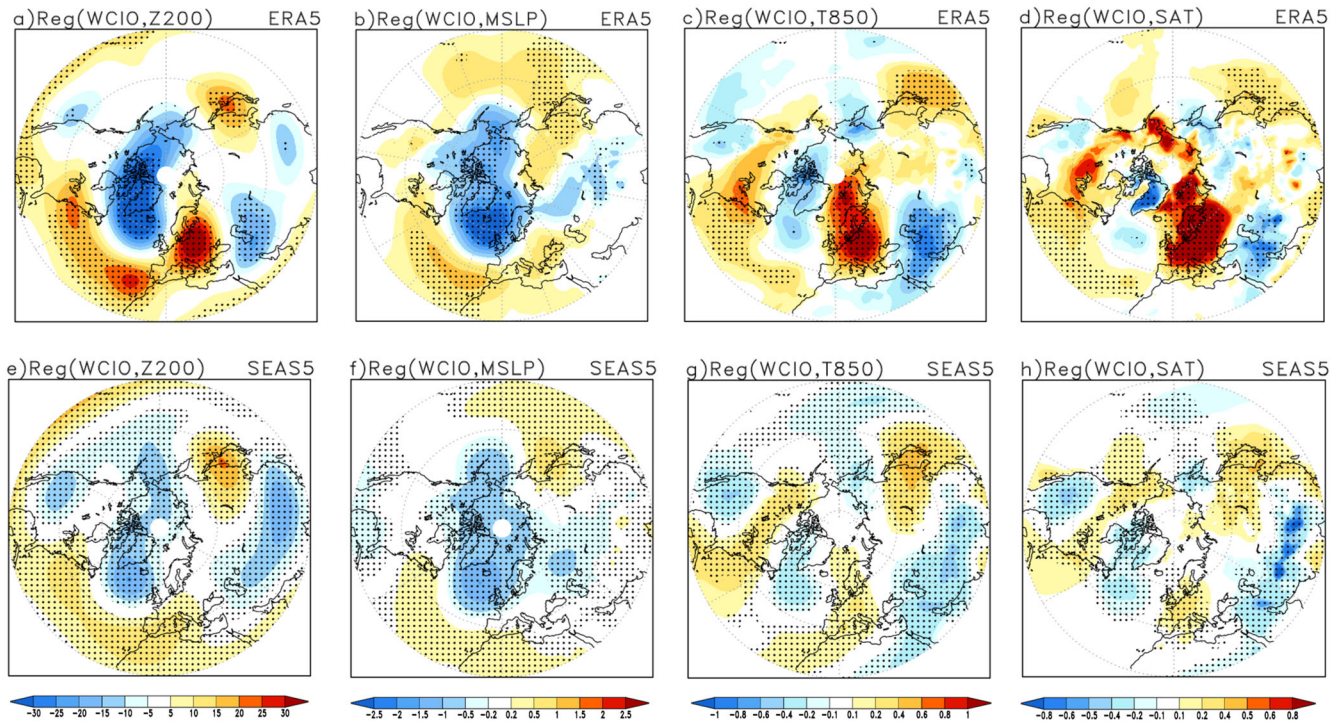
Fig. 4 Indian Ocean teleconnections to the North Atlantic European Region. a Observed Regression of the early winter (November–December; ND) WCIO precipitation anomalies index with the early winter (ND) 200-hPa geopotential height anomalies (Units; m) for the period 1981–2019; (**b**) same as of (**a**) but with Mean Sea Level Pressure (Units; hPa); (**c**) same as of (**a**) but for 850-hPa temperature anomalies (Units; K); (**d**) same as of (**a**) but for the Surface Air Temperature (Units; K) (**e**–**h**) Same as (**a**–**d**) but for ECMWF-SEAS5 dataset. Stippling denotes statistical significance at 95% confidence level. The observed (ECMWF-SEAS5) Correlation Coefficient (CC) between NAO index and WCIO is 0.44 (0.64), while with Niño3.4 is 0.42 (0.57), statistically significant at 95% confidence level.

reproduced in the model (Fig. 4h) compared to the observations (Fig. 4d). The weaker response of the Arctic circle temperature to the Indian Ocean in SEAS5 compared to ERA5, may be due to differences in the sea-ice cover. Furthermore, we defined the observed NAO index, using 200-hPa geopotential regressions (Fig. 4a), as the difference between the Azores [26:40 °N; 310:360 °E] and Iceland [50:80 °N; 310:350 °E] (boxes highlighted in Supplementary Fig. 3) and found a slightly higher statistically significant (95% confidence level) Correlation Coefficient (CC) with WCIO index (0.44) compared to the Niño34 index (0.42). Similarly, for ECMWF-SEAS5, the CC of NAO with WCIO is 0.64, while with Niño34 is 0.57 (both are statistically significant at 95% confidence level), indicating a similar behavior as in observations. In order to investigate if the modeled WCIO response in the North Atlantic region is consistent in magnitude with the observed one, we calculated the NAO index (boxes highlighted in Supplementary Fig. 3) from the 200-hPa regression onto the WCIO anomalies for each ensemble member and compared with the observations (Supplementary Fig. 4). No ensemble member captures the observed value, which is located at about 2 standard deviations of the ensemble mean value. Next, we analyze the predictability of the tropical WCIO precipitation and NAE circulation anomalies during the early winter based on the October initial conditions.

Predictability of the Western-Central Indian Ocean and North Atlantic circulation anomalies

The predictability of the early winter precipitation anomalies over the tropical WCIO are assessed using the actual and the potential predictability matrix (see "methods"). Figure 5a shows a maximum of the actual prediction skill over the western-central Indian Ocean, while other maxima are noted in the southeastern half of the Indian Ocean near Java and Sumatra region, which coincides well with the spatiotemporal pattern of the potential predictability

(Fig. 5b), indicating that the model re-forecast is well calibrated. Figure 5c compares observed WCIO precipitation anomaly index with the model ensemble (mean and individual members), where the prediction skill between the model ensemble mean and GPCP is 0.66, while with ERA5, it is 0.72. Apart from very few years, the observation lies within the spread of the model ensemble members. Moreover, the prediction skill remains large (0.68) after removing ENSO, while it drops significantly (0.39) after removing IOD.

Figure 6a shows the map of temporal anomaly correlation of the observed 200-hPa geopotential height anomalies with the ECMWF ensemble mean anomalies in the northern hemisphere. Predictability typically decreases from the tropical to extratropical regions due to the dominance of noise in extratropical regions[33,52]. A significant actual prediction skill is noted southeast of Greenland in the North Atlantic region where the skill exceeds 0.6 and represents the largest value north of 50° N, which is even larger than the prediction skill of the PNA region. A prominent actual prediction skill is also noted over the western and central European continental region. Prediction skill over the PNA region is typically attributed to ENSO teleconnections[33], but the ENSO teleconnections during early winter are relatively weak to the PNA region[53], compared to the NAE region[32,39,53,54], which may result in the higher prediction skill for the North Atlantic sector (Fig. 6a). However, recent studies show that early winter ENSO teleconnections to NAE are mainly mediated through the Indian Ocean[7,8], and the tropical North Atlantic region[40,55]. This is also consistent with the stronger teleconnection in the NAE region from the WCIO precipitation anomalies (Fig. 4a, b). Moreover, the spatial pattern of the potential predictability is similar to the actual prediction skill (Fig. 6b).

We also investigated the relative strength of predictability during early winter over NAE region using the Ratio of the
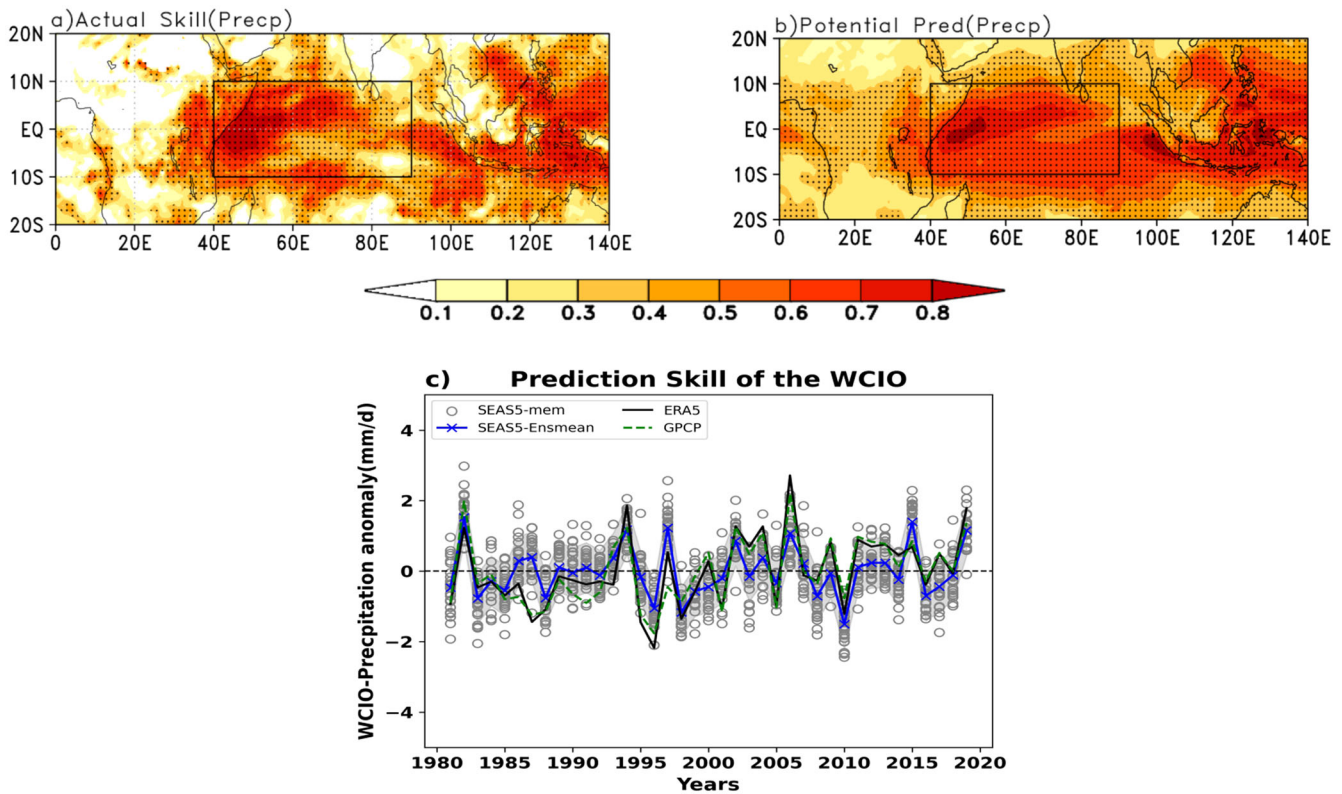
Fig. 5 Prediction skill of the WCIO precipitation anomalies. a Actual Prediction skill of the early winter (November–December; ND) precipitation anomalies over the tropical western-central Indian Ocean (WCIO) [40:90°E; 10°S:10°N] region; (b) Potential Predictability of the WCIO precipitation anomalies. Stippling denotes statistical significance at 95% confidence level; (c) Prediction skill of the early winter (ND) precipitation anomalies over the WCIO region with respect to ERA5(GPCP) is 0.72(0.66). Grey circles show each ensemble member for ECMWF-SEAS5, while blue line is the SEAS5 ensemble mean, black line represents ERA5 and green dashed line is for GPCP. Light grey shading is the ensemble mean spread based on its 1-sigma level.

Predictable Component (RPC)[48] matrix. In Fig. 6c, regions with RPC greater than 1 (underconfident) indicate the occurrence of signal-to-noise paradox, because it violates the expectation of an overconfident model behaviour in these locations. A higher potential predictability is noted over the western European region compared to the actual prediction skill and thus the RPC less than 1, while southeast of Greenland a larger actual prediction skill is noted compared to the potential predictability, and thus RPC is larger than 1, indicating the signal-to-noise paradox. A plausible explanation for these regions with RPC > 1 for the early winter season (ND) is that the model response from the Indian Ocean (Fig. 4e, f) is weaker than the observed (Fig. 4a, b). Indeed the magnitudes of the NAO response in individual ensemble members to Indian Ocean precipitation anomalies are inconsistent with the observed one (Supplementary Fig. 4). Another possible factor contributing to under-confident regions (RPC > 1) could be weak transient eddy feedbacks in the model[56].

Figure 7 shows the actual prediction skill and potential predictability of the NAO index based on 200-hPa geopotential height anomalies (boxes highlighted in Supplementary Fig. 3) during early boreal winter season. NAO shows an actual prediction skill of 0.36, whereas its potential predictability is 0.33 (both are statistically significant at 95% confidence level), consistent with the signal-to-noise paradox noted in Fig. 6. To show that the results do not strongly depend on the field used for NAO definition, we also defined the NAO index (boxes highlighted in Supplementary Fig. 3) based on MSLP, and found that the main results do not change. The MSLP based NAO actual prediction skill is 0.34, and due to the large spread among the members, a low signal-to-noise ratio is noted that results into the moderate NAO potential predictability of 0.13, which is lower compared to that of NAO based on 200-hPa geopotential height anomalies. After linearly removing the Indian Ocean (WCIO) influence from 200-hPa geopotential height anomalies (see methods), the actual prediction skill of the residual NAO index (NAO_noWCIO) computed from the residual 200-hPa geopotential height anomalies reduces to 0.13 while the potential predictability is 0.20. Similarly, if the Niño34 index is linearly removed, the residual NAO actual prediction skill (NAO_noNiño34) drops to 0.24, and the potential predictability to 0.25 (Fig. 7). It implies that NAO shows a skillful prediction due to constructive interference between ENSO and Indian Ocean, where the Indian Ocean dominates, consistent with earlier findings[6,7,57].

The positive WCIO precipitation anomalies lead to milder early winter temperature conditions over the European region (Fig. 4d). Now, does the model have an ability to predict the early winter SAT conditions? To answer this question, we investigated the prediction skill of the Surface Air Temperature (SAT) over the NAE region. Figure 8a, b compares the actual prediction skill of the SAT with the potential predictability over the NAE region during the early winter. A statistically significant actual prediction skill of the SAT is noted over the southern U.K., and western Europe with a maximum over France, and Germany including parts of the Scandinavian region (Fig. 8a), which coincides overall well with the potential predictability over the NAE region (Fig. 8b). Whilst the western and the northwestern European region show a higher potential predictability, mostly over the oceans, (Fig. 8b) compared to the actual prediction skill (Fig. 8a). While SAT predictability is largely confined to the North Atlantic Ocean region, likely due to the large thermal inertia, also an increased surface temperature predictability is noted in the western
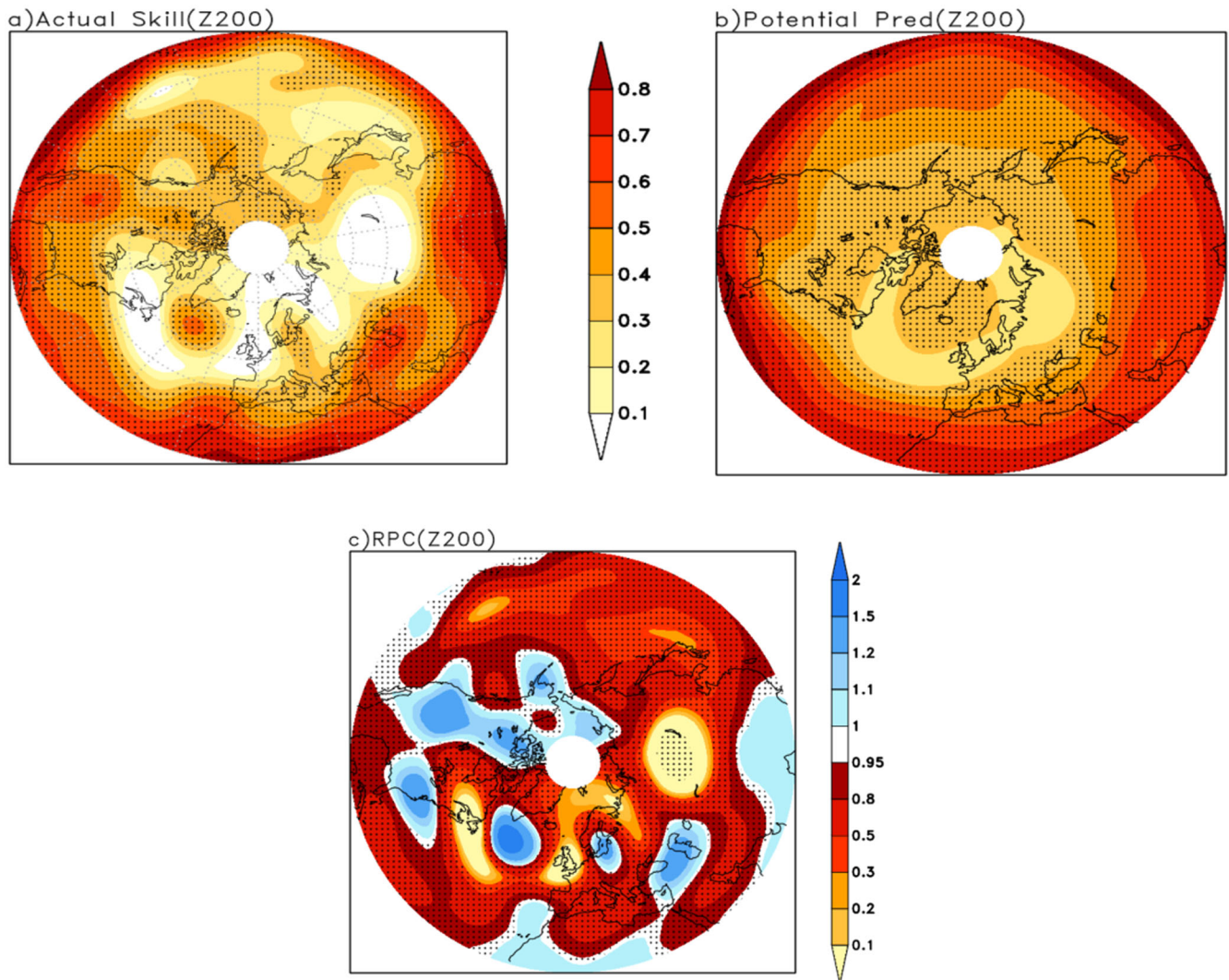
Fig. 6 Predictability of the North Atlantic European circulation anomalies. a Actual prediction skill of the early winter (November–December; ND) 200-hPa geopotential height anomalies (Z200) over the North Atlantic European (NAE) region; (**b**) Potential Predictability of the 200-hPa geopotential height anomalies over NAE region; (**c**) Ratio of the Predictable Component (RPC), where RPC > 1 shows under confidence behavior of the model (blue), while RPC < 1 is the overconfident behavior (red). Stippling denotes the statistical significance at 95% confidence level.

European region, as discussed above (Fig. 8c). Overall, 0.52 temperature prediction skill is noted over the western European [0:20 °E; 45:55 °N] region. Such a prominent statistically significant predictability is likely related to a predictability in low-level zonal winds that may change the advection of warmer air from the Ocean to the European continent[51]. Indeed, as shown in Fig. 8c, the zonal wind at 850-hPa (Uwnd850) shows a significant potential predictability south of the U.K. These dynamical and thermal features in the predictability are all consistent with the signals induced by the teleconnections from the Indian Ocean (Fig. 4), which is providing a plausible signal for the modulation of the prediction skill over the NAE region.

DISCUSSION

In this study we found that the tropical WCIO precipitation anomalies modulate the NAE circulation anomalies during the early winter in observations as well as in ECMWF-SEAS5 re-forecast system. We found that the boreal autumn IOD pre-conditioning is the dominating mechanism that triggers the precipitation

anomalies in the WCIO region during early winter, which are further enhanced by the ENSO forcing through a direct atmospheric bridge in early winter (Figs. 2, 3). However, a part of the autumn IOD is forced by the developing ENSO event.

The precipitation anomalies in the Indian Ocean are skillfully predicted in the ECMWF-SEAS5 prediction system. A statistically significant (95% confidence level) prediction skill (0.72) is noted for the tropical WCIO precipitation anomalies during the boreal early winter. The spatial distribution of actual prediction skill in the Indian Ocean resembles closely to the potential predictability, indicating a good calibration of the precipitation forecasts for this region. Moreover, the actual prediction skill of the WCIO precipitation anomaly with linearly removed ENSO [i.e., WCIO_-noENSO] drops to 0.68, while after removing IOD linearly, it drops to 0.39, indicating that the pre-conditioning of the IOD is the dominant mechanism to excite the early winter IO precipitation anomalies. It also shows that the constructive interference between ENSO and IOD enhances the prediction skill of the WCIO precipitation anomalies. These WCIO precipitation, or equivalently, heating anomalies are the Rossby wave sources for
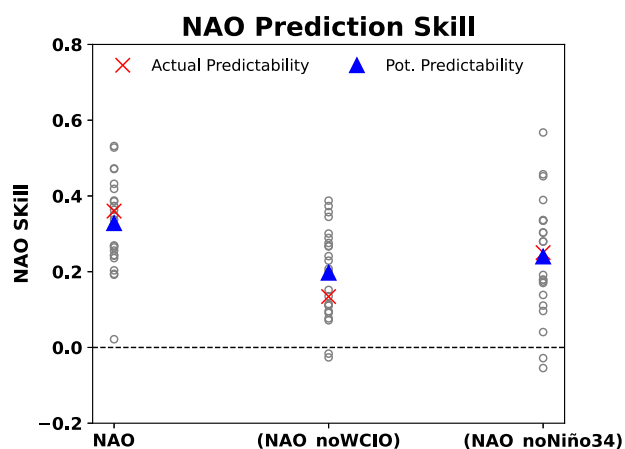
Fig. 7 NAO prediction skill. Prediction skill of the North Atlantic Oscillation (NAO) index [26:40 °N; 310:360 °E - 50:80 °N; 310:350 °E] estimated based on the 200-hPa geopotential height anomalies during early winter (November–December; ND). The grey open circle is the potential predictability for each member and the average of the 25 correlations is the potential predictability (blue triangle) of the model compared with actual prediction skill (red cross). NAO means total Skill, while NAO_noWCIO means ENSO residual signal after removing WCIO anomalies and vice-versa for the NAO_noNiño34.

the Indian Ocean teleconnection to North Atlantic region during the early winter season[7,27]. The positive relationship (CC; 0.44) between the WCIO and NAO shows that a positive WCIO precipitation anomaly favors a positive phase of NAO, that leads to milder surface temperature conditions in the western European region. These features are overall well reproduced by the ECMWF-SEAS5, but with weaker amplitude. Also, a notable spatial actual prediction skill of the atmospheric circulation anomalies appears in the North Atlantic region southeast of Greenland as well as over the European continent. Overall, during early winter prediction skill of NAO is 0.36 (Fig. 7), while for the surface temperatures over the western Europe it is 0.52 (Fig. 8a), which is dominated by the Indian Ocean signals through its teleconnections[7,8].

This study highlights the importance of the correct representation of Indian Ocean precipitation anomalies, its teleconnections to the North Atlantic region, and the European climate in the seasonal forecasting systems. It also shows that for the assessment of predictability in extratropical regions, particularly for the NAE region, the sub-seasonal changes of inter-basin teleconnections should be considered, when choosing the target prediction months. This is because of the dominance of the positive NAO like response to positive Indian Ocean precipitation anomalies identified for early winter, which co-occur with warm ENSO conditions. In late winter, on the other hand, the response in the NAE region is dominated by direct ENSO forcing, and resembles more negative NAO-like condition[7,8,37,39].
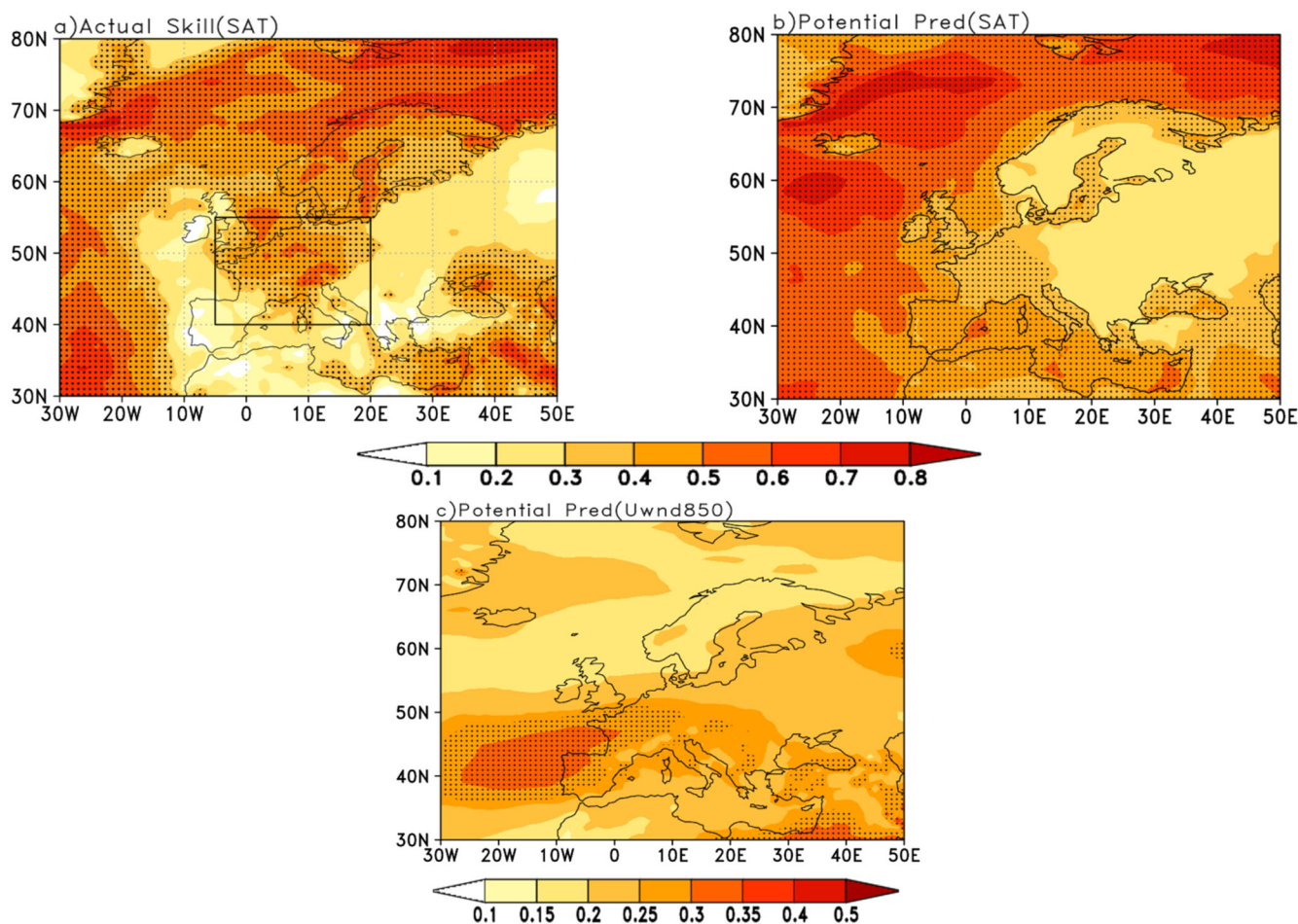

Fig. 8 Prediction skill of the temperature and winds in the North Atlantic European region. a Actual prediction skill of the early winter (November–December; ND) Surface Air Temperature (SAT) anomalies over the North Atlantic European (NAE) region for the period 1981–2019; (**b**) Potential Predictability of the SAT over the NAE region for the same period. Stippling denotes statistical significance at 95% confidence level. The Prediction skill of the SAT over the western European region [0:20 °E; 45:55 °N] is 0.52. **c** Same as of (**b**) but for 850-hPa zonal winds (Uwnd850) anomalies. Stippling denotes statistical significance at 90% confidence level.

METHODS

Datasets

The European Centre for Medium-Range Weather Forecasts seasonal prediction system (ECMWF-SEAS5)[19] re-forecast dataset is based on the Integrated Forecast System (IFS) atmospheric model coupled to the Nucleus for Oceanic Modeling of the Ocean (NEMO) v4.5 ocean model. The atmospheric model horizontal resolution is T319 having 91 vertical levels, with a model top at 0.01 hPa. The coupled system includes the Louvian-la-Neuve Sea Ice Model (LIM2) with ORCA 0.25° resolution and a wave model at 0.5°. For each year, ERA-Interim atmospheric initial conditions are used, while the Ocean Reanalysis System 5 (ORAS5) was used for the ocean initialization. The land, soil and snow initializations were made based on the forced 43r1 land surface model. A total of 25 ensemble members are available for the period 1981–2016, with each member starting from the first day of October, available at 1° × 1° resolution from the Copernicus Climate Change Service portal (https://climate.copernicus.eu). Moreover, we extended the analysis using the forecast data for the period 2017–2019 with 25-ensemble members for the similar (1st October) initial conditions. The focus is to analyse the prediction skill of the precipitation anomalies in the Tropical Indian Ocean and that of North Atlantic European (NAE) circulation anomalies during the early winter based on October Initial conditions. To eliminate the influence of the initial conditions on the predictability, October was excluded and the analysis is focused on the late fall to early half of the boreal winter season (i.e., November–December; ND).

The fifth generation European Re-Analysis (ERA5)[58] dataset at higher horizontal (0.25° × 0.25°) and the vertical resolution was adapted as proxy to the observed/reanalysis dataset to analyse the observed teleconnections patterns and predictability. Moreover, the Global Precipitation dataset namely as the Global Precipitation Climatology Project (GPCP) at 2.5° × 2.5° horizontal grid spacing was also adapted as the observed precipitation dataset, which is mainly based on the surface gauges, sounding and satellite observations[59]. The observed and reanalysis dataset were re-gridded to the 1° × 1° horizontal resolution. We noted, the prediction skill of the WCIO precipitation anomalies is robust irrespective of the observed and reanalysis precipitation dataset.

Methodology

Linear regression is defined as the covariance of the standardized anomaly index to the field of interest. Furthermore, the Partial regression analysis[50] is adapted to isolate the tropical signals statistically from each other using Eq. (1).

$$X_{res}(t) = X(t) - b(x, y) \times X(t)_{rm} \qquad (1)$$

In Eq. (1), $b(x, y)$ is the regression coefficient of the forcing to be removed $(X(t)_{rm})$ from the original $(X(t))$ that results into the residual $X_{res}(t)$ time series statistically.

The model's predictability is assessed through the actual and potential predictability matrix. The actual prediction skill is defined as the point-by-point temporal anomaly correlation between the observation and the model ensemble mean, while Potential Predictability is defined as the square root of the signal to the total (signal and noise) variances also known as the theoretical limit of the correlation skill. Signal variance is defined as the variance of the ensemble mean anomalies, while variance of the ensemble deviation from the ensemble mean is known as the noise variance[52,60]. The ratio of the actual prediction skill to the potential predictability defines the Ratio of the Predictable Component (RPC)[48,61]. Moreover, the perfect model potential predictability (PP) is used to examine the NAO predictability (Fig. 7), where NAO index of each member is correlated with the ensemble mean of the $N - 1$ (remaining members), which is known to be an estimation of the model's skill to predict itself[48].

This procedure is repeated for N members, and the average correlation obtained from the N correlations using the fisher Z-transformation defines the perfect model correlation skill for the NAO index[48].

A two-tailed t-test was used to analyze the statistical significance of the results, while the standard deviation derived from the inter-ensemble spread is used to analyze the significance of the ECMWF-SEAS5 regression maps.

REFERENCES

1. Hurrell, J. W., Kushnir, Y. & Visbeck, M. The North Atlantic Oscillation. *Sci. (80-.)* **291**, 603–605 (2001).
2. Hurrell, J. W., Hoerling, M. P., Phillips, A. S. & Xu, T. Twentieth century north atlantic climate change. Part I: assessing determinism. *Clim. Dyn.* **23**, 371–389 (2004).
3. Hu, S. & Fedorov, A. V. Indian Ocean warming as a driver of the North Atlantic warming hole. *Nat. Commun.* https://doi.org/10.1038/s41467-020-18522-5 (2020).
4. Hurrell, J. W. Decadal trends in the North Atlantic oscillation: regional temperatures and precipitation. *Sci. (80-.)* **269**, 676–679 (1995).
5. Bader, J. & Latif, M. North Atlantic oscillation response to anomalous Indian ocean SST in a coupled GCM. *J. Clim.* **18**, 5382–5389 (2005).
6. Hardiman, S. C. et al. Predictability of European winter 2019/20: Indian Ocean dipole impacts on the NAO. *Atmos. Sci. Lett.* **21**, 1–10 (2020).
7. Abid, M. A. et al. Separating the Indian and Pacific Ocean impacts on the Euro-Atlantic response to ENSO and its transition from early to late winter. *J. Clim.* **34**, 1531–1548 (2021).
8. Joshi, M. K., Abid, M. A. & Kucharski, F. The role of an Indian Ocean heating dipole in the ENSO teleconnection to the North Atlantic European region in early winter during 20th century in Reanalysis and CMIP5 simulations. *J. Clim.* **34**, 1047–1060 (2021).
9. Cai, W. et al. Pantropical climate interactions. *Sci. (80-.)* **363**, eaav4236 (2019).
10. Interacting Climates of Ocean Basins. (Cambridge University Press, 2020). https://doi.org/10.1017/9781108610995.
11. Wang, C. Three-ocean interactions and climate variability: a review and perspective. *Clim. Dyn.* **53**, 5119–5136 (2019).
12. Ding, R. et al. The internal and ENSO-forced modes of the Indian Ocean sea surface temperature. *J. Clim.* 1–49 https://doi.org/10.1175/JCLI-D-21-0403.1 (2022).
13. Ashok, K., Guan, Z. & Yamagata, T. Impact of the Indian Ocean dipole on the relationship between the Indian monsoon rainfall and ENSO. *Geophys. Res. Lett.* **28**, 4499–4502 (2001).
14. Ashok, K., Guan, Z. & Yamagata, T. Influence of the Indian Ocean Dipole on the Australian winter rainfall. *Geophys. Res. Lett.* **30**, 1821 (2003).
15. Cai, W., Van Rensch, P., Cowan, T. & Hendon, H. H. An asymmetry in the IOD and ENSO teleconnection pathway and its impact on Australian climate. *J. Clim.* **25**, 6318–6329 (2012).
16. Yang, J., Liu, Q., Liu, Z., Wu, L. & Huang, F. Basin mode of Indian Ocean sea surface temperature and Northern Hemisphere circumglobal teleconnection. https://doi.org/10.1029/2009GL039559 (2009).
17. Saji, N., Goswami, B., Vinayachandran, P. & Yamagata, T. A dipole mode in the Tropical Ocean. *Nature* **401**, 360–363 (1999).
18. Yang, Y. et al. Seasonality and predictability of the Indian Ocean dipole mode: ENSO forcing and internal variability. *J. Clim.* **28**, 8021–8036 (2015).

19. Wang, G. & Cai, W. Two-year consecutive concurrences of positive Indian Ocean Dipole and Central Pacific El Niño preconditioned the 2019/2020 Australian "black summer" bushfires. *Geosci. Lett.* **7**, 19 (2020).

20. Lee, R. W., Woolnough, S. J., Charlton-Perez, A. J. & Vitart, F. ENSO modulation of MJO teleconnections to the North Atlantic and Europe. *Geophys. Res. Lett.* **46**, 13535–13545 (2019).

21. Wu, Y. & Tang, Y. Seasonal predictability of the tropical Indian Ocean SST in the North American multimodel ensemble. *Clim. Dyn.* **53**, 3361–3372 (2019).

22. Shi, L. et al. How predictable is the indian ocean dipole? *Mon. Weather Rev.* **140**, 3867–3884 (2012).

23. Johnson, S. J. et al. SEAS5: The new ECMWF seasonal forecast system. *Geosci. Model Dev.* **12**, 1087–1117 (2019).

24. Vitart, F. & Molteni, F. Simulation of the Madden-Julian Oscillation and its tele-connections in the ECMWF forecast system. *Q. J. R. Meteorol. Soc. Q. J. R. Meteorol. Soc.* **136**, 842–855 (2010).

25. Molteni, F., Stockdale, T. N. & Vitart, F. Understanding and modelling extra-tropical teleconnections with the Indo-Pacific region during the northern winter. *Clim. Dyn.* **45**, 3119–3140 (2015).

26. Vitart, F. Madden—Julian Oscillation prediction and teleconnections in the S2S database. *Q. J. R. Meteorol. Soc.* **143**, 2210–2220 (2017).

27. Molteni, F. et al. *Boreal-winter teleconnections with tropical Indo-Pacific rainfall in HighResMIP historical simulations from the PRIMAVERA project. Climate Dynamics* vol. 55 (Springer Berlin Heidelberg, 2020).

28. Fletcher, C. G. & Kushner, P. J. The role of linear interference in the annular mode response to tropical SST forcing. *J. Clim.* **24**, 778–794 (2011).

29. Mathieu, P.-P., Sutton, R. T., Dong, B. & Collins, M. Predictability of winter climate over the North Atlantic European region during ENSO events. *J. Clim.* **17**, 1953–1974 (2004).

30. Deser, C. & Phillips, A. S. Atmospheric circulation trends, 1950–2000: the relative roles of sea surface temperature forcing and direct atmospheric radiative forcing. *J. Clim.* **22**, 396–413 (2009).

31. Brönnimann, S. Impact of El Niño-Southern Oscillation on European climate. *Rev. Geophys.* **45**, RG3003 https://doi.org/10.1029/2006RG000199 (2007).

32. King, M. P., Li, C. & Sobolowski, S. Resampling of ENSO teleconnections: accounting for cold-season evolution reduces uncertainty in the North Atlantic. *Weather Clim. Dyn.* **2**, 759–776 (2021).

33. Deser, C., Simpson, I. R., Phillips, A. S. & McKinnon, K. A. How well do we know ENSO's climate impacts over North America, and how do we evaluate models accordingly? *J. Clim.* **31**, 4991–5014 (2018).

34. Toniazzo, T. & Scaife, A. A. The influence of ENSO on winter North Atlantic climate. *Geophys. Res. Lett.* **33**, 24704 (2006).

35. Ivasić, S., Herceg-Bulić, I. & King, M. P. Recent weakening in the winter ENSO teleconnection over the North Atlantic-European region. *Clim. Dyn.* **57**, 1953–1972 (2021).

36. Scaife, A. A. et al. Skillful long-range prediction of European and North American winters. *Geophys. Res. Lett.* **41**, 2514–2519 (2014).

37. Scaife, A. A. et al. Tropical rainfall, Rossby waves and regional winter climate predictions. *Q. J. R. Meteorol. Soc.* **143**, 1–11 (2017).

38. Jiménez-Esteve, B. & Domeisen, D. I. V. The tropospheric pathway of the ENSO–North Atlantic teleconnection. *J. Clim.* **31**, 4563–4584 (2018).

39. King, M. P. et al. Importance of late fall ENSO teleconnection in the euro-atlantic sector. *Bull. Am. Meteorol. Soc.* **99**, 1337–1343 (2018).

40. Ayarzagüena, B., Ineson, S., Dunstone, N. J., Baldwin, M. P. & Scaife, A. A. Intra-seasonal effects of El Niño-Southern Oscillation on North Atlantic climate. *J. Clim.* **31**, 8861–8873 (2018).

41. Mezzina, B., García-Serrano, J., Bladé, I. & Kucharski, F. Dynamics of the ENSO teleconnection and NAO variability in the North Atlantic–European late winter. *J. Clim.* **33**, 907–923 (2020).

42. Ineson, S. & Scaife, A. A. The role of the stratosphere in the European climate response to El Niño. *Nat. Geosci.* **2**, 32–36 (2009).

43. Domeisen, D. I. V. et al. Seasonal predictability over Europe Arising from El Niño and stratospheric variability in the MPI-ESM seasonal prediction system. *J. Clim.* **28**, 256–271 (2015).

44. Domeisen, D. I. V., Garfinkel, C. I. & Butler, A. H. The teleconnection of El Niño Southern Oscillation to the Stratosphere. *Rev. Geophys.* **57**, 5–47 (2019).

45. Lu, B. & Ren, H. L. What caused the extreme Indian Ocean dipole event in 2019? *Geophys. Res. Lett.* **47**, 8 (2020).

46. Hardiman, S. C. et al. The impact of strong El Niño and La Niña Events on the North Atlantic. *Geophys. Res. Lett.* **46**, 2874–2883 (2019).

47. Trascasa-Castro, P., Maycock, A. C., Yiu, Y. Y. S. & Fletcher, J. K. On the linearity of the stratospheric and euro-atlantic sector response to ENSO. *J. Clim.* **32**, 6607–6626 (2019).

48. Scaife, A. A. & Smith, D. A signal-to-noise paradox in climate science. *npj Clim. Atmos. Sci.* **1**, 28 (2018).

49. Abid, M. A., Ashfaq, M., Kucharski, F., Evans, K. J. & Almazroui, M. Tropical Indian Ocean mediates ENSO influence over central Southwest Asia during the wet season. *Geophys. Res. Lett.* **47**, e2020GL089308. https://doi.org/10.1029/2020GL089308 (2020).

50. Cai, W., van Rensch, P., Cowan, T. & Hendon, H. H. Teleconnection pathways of ENSO and the IOD and the mechanisms for impacts on Australian rainfall. *J. Clim.* **24**, 3910–3923 (2011).

51. Clark, J. P. & Feldstein, S. B. What drives the North Atlantic Oscillation's temperature anomaly pattern? Part I: the growth and decay of the surface air temperature anomalies. *J. Atmos. Sci.* **77**, 185–198 (2020).

52. Abid, M. A., Kang, I. S., Almazroui, M. & Kucharski, F. Contribution of synoptic transients to the potential predictability of PNA circulation anomalies: El niño versus la niña. *J. Clim.* **28**, 8347–8362 (2015).

53. Bladé, I., Newman, M., Alexander, M. A. & Scott, J. D. The late fall extratropical response to ENSO: sensitivity to coupling and convection in the tropical west Pacific. *J. Clim.* **21**, 6101–6118 (2008).

54. King, M. P., Herceg-Bulić, I., Kucharski, F. & Keenlyside, N. Interannual tropical Pacific sea surface temperature anomalies teleconnection to Northern Hemisphere atmosphere in November. *Clim. Dyn.* **50**, 1881–1899 (2018).

55. Casselman, J. W., Taschetto, A. S. & Domeisen, D. I. V. Nonlinearity in the pathway of El Niño–Southern Oscillation to the Tropical North Atlantic. *J. Clim.* **34**, 7277–7296 (2021).

56. Hardiman, S. C. et al. Missing eddy feedback may explain weak signal-to-noise ratios in climate predictions. *npj Clim. Atmos. Sci.* **5**, 57 (2022).

57. Fletcher, C. G. & Cassou, C. The dynamical influence of separate teleconnections from the Pacific and Indian Oceans on the Northern Annular Mode. *J. Clim.* **28**, 7985–8002 (2015).

58. Hersbach, H. et al. The ERA5 global reanalysis. *Q J. R. Meteorol. Soc.* **146**, 1999–2049 (2020).

59. Adler, R. F. et al. The Global Precipitation Climatology Project (GPCP) Monthly Analysis (New Version 2.3) and a Review of 2017 Global Precipitation. https://doi.org/10.3390/atmos9040138.

60. Kang, I.-S., Kug, J.-S., Lim, M.-J. & Choi, D.-H. Impact of transient eddies on extratropical seasonal-mean predictability in DEMETER models. *Clim. Dyn.* **37**, 509–519 (2011).

61. Eade, R. et al. Do seasonal-to-decadal climate predictions underestimate the predictability of the real world? *Geophys Res Lett.* https://doi.org/10.1002/2014GL061146 (2014).

ACKNOWLEDGEMENTS

AUTHOR CONTRIBUTIONS

The concept was discussed between M.A.A, F.K. and F.M. M.A.A. lead the work including the data collection, analysis, writing and revisions. F.K. and F.M. contributed to the writing and discussions. M.A. contributed to the discussions.

COMPETING INTERESTS

The authors declare no competing interests.

ADDITIONAL INFORMATION

Supplementary information The online version contains supplementary material available at https://doi.org/10.1038/s41612-023-00328-z.

Correspondence and requests for materials should be addressed to Muhammad Adnan Abid.

Reprints and permission information is available at http://www.nature.com/reprints